
Article:
Wagg, D.J. and Bishop, S.R. (2001) Chatter, sticking and chaotic impacting motion in a two-degree of freedom impact oscillator. International Journal of Bifurcation and Chaos, 11. 57 - 71. ISSN 0218-1274

https://doi.org/10.1142/S0218127401001943

International Journal of Bifurcation and Chaos, Vol. 11, No. 1 (2001) 57–71

CHATTER, STICKING AND CHAOTIC IMPACTING MOTION IN A TWO-DEGREE OF FREEDOM IMPACT OSCILLATOR

D. J. Wagg* and S. R. Bishop

Department of Mechanical Engineering, University of Bristol, Queens Building, University Walk, Bristol BS8 1TR, U.K.

March 7,2000

Abstract

We consider the dynamics of a two degree of freedom impact oscillator subject to a motion limiting constraint. These systems exhibit a range of periodic and non-periodic impact motions. For a particular set of parameters, we consider the bifurcations which occur between differing regimes of impacting motion and in particular those which occur due to a grazing bifurcation. Unexpected resonant behaviour is also observed, due to the complexity of the dynamics. We consider both periodic and chaotic chatter motions and the regions of sticking which exist. Finally we consider the types of chaotic motion that occur within the parameter range. We discuss the possibility in relating successive low velocity impacts, especially in respect to possible low dimensional mappings for such a system.

Running title:A two-degree of freedom impact oscillator

*Current address: Earthquake Engineering Research Centre, Department of Civil Engineering, University of Bristol, Queens Building, University Walk, Bristol BS8 1TR, U.K. David.Wagg@bristol.ac.uk

International Journal of Bifurcation and Chaos, Vol. 11, No. 1 (2001) 57–71

1 Introduction

In this paper we consider the dynamics of a two degree of freedom impact oscillator. This system belongs to a wider class of multi-degree of freedom impact oscillators. We define such a multi-degree of freedom impact oscillator as a system of coupled masses, where the motion of one mass is restricted by an impact stop. Non-impacting multi-degree of freedom (lumped mass) systems are used extensively to model engineering systems (Bishop & Johnson 1960; Timoshenko *et al.* 1974). Two-degree of freedom impact oscillators have been studied in relation to impact damper systems (Masri 1972; Chatterjee *et al.* 1995), which are essentially a two degree of freedom system with a primary mass and an additional impacting mass. The two-degree of freedom impact oscillator has also been considered by Shaw & Shaw (1989), who studied bifurcations, and the onset of chaotic motion in such systems, while Neilson & Gonsalves (1993) considered the dynamics of rotor bearings using a two degree of freedom model.

The effect of an impact damper on a multi-degree of freedom system has been considered by Nigm & Shabana (1983). Higher degree of freedom impact systems have also been considered by Cusumano & Bai (1993), who consider the dynamics associated with a ten degree of freedom impact oscillator. Periodic impacting motions which occur in multi-degree of freedom impact systems have also been investigated. Natsiavas (1993) has generalised the method for finding periodic $\mathbf{P}(p, q)$ orbits developed by Shaw & Holmes (1983), to N degree of freedom impact oscillators. This method employs a root finding method to locate the time of impact for the periodic orbit. More recently Pun *et al.* (1998) have considered the type of $\mathbf{P}(p, q)$ motions which occur in a constrained multi-degree of freedom impact oscillator, using a two degree of freedom example.

In this current work we also consider a two degree of freedom impact oscillator, but focus our attention on nonsmooth phenomena such as chatter and sticking, which have not been previously considered in detail for such a system. In addition, we present simulations of chaotic attractors for the two degree of freedom system. In particular we consider the form of the attractor close to a grazing bifurcation (Nordmark 1991). By examining the relationship between successive low velocity impacts in these attractors, we discuss the possibility of modelling the system using low dimensional mapping. These results are compared with those of Fredriksson & Nordmark (1997) who consider localised mappings for multi-degree of freedom impacting systems.

2 Mathematical model

Initially we consider a generalised N degree of freedom coupled linear oscillator system with N lumped masses. A schematic representation of such a model is shown in Fig. 1. The equations of motion for the coupled masses can be expressed as

$$m_i\ddot{x}_i + c_i(\dot{x}_i - \dot{x}_{i-1}) + c_{i+1}(\dot{x}_i - \dot{x}_{i+1}) + k_i(x_i - x_{i-1}) + k_{i+1}(x_i - x_{i+1}) = f_i(t), \tag{1}$$

for $i = 1, 2 \ldots, N-1$ and

$$m_N\ddot{x}_N + c_N(\dot{x}_N - \dot{x}_{N-1}) + k_N(x_N - x_{N-1}) = f_N(t) \tag{2}$$

for $i = N$ (Gladwell 1986). Here x_i represents the displacement of mass m_i, an overdot is used to represent differentiation with respect to time t and $f_i(t)$ represents the forcing function for the ith degree of freedom. These expressions govern the motion while the displacement x_N is less than some fixed value x_s corresponding to the position of an impact stop. When $x_N = x_s$ an impact occurs. This impact is modelled using an instantaneous coefficient of restitution rule such that

$$\dot{x}_N(t_+) = -r\dot{x}_N(t_-) \tag{3}$$

where, t_- is the time just before impact, t_+ is the time just after impact and r is the coefficient of restitution with a value in the range $r \in [0, 1]$. For this system we assume that only mass m_N can impact.

The equations of motion for the coupled masses can be expressed in matrix form as

$$[M]\ddot{\mathbf{x}} + [C]\dot{\mathbf{x}} + [K]\mathbf{x} = \mathbf{f}(t) \quad x_N < x_s \tag{4}$$

where $[M], [C], [K]$ are the mass, damping and stiffness matrices respectively, $\mathbf{x} = \{x_1, x_2 \ldots, x_N\}^T$ the displacement vector and $\mathbf{f}(t) = \{f_1, f_2 \ldots, f_N\}^T$ the external forcing vector. The coupling between masses occurs via the matrices $[C]$ and $[K]$, which are nondiagonal (although usually banded). The mass matrix $[M]$ is a diagonal matrix.

In matrix form the coefficient of restitution rule is

$$\dot{\mathbf{x}}(t_+) = [R]\dot{\mathbf{x}}(t_-) \quad x_N = x_s \tag{5}$$

where $[R]$ is the $N \times N$ matrix

$$[R] = \begin{bmatrix} 1 & 0 & 0 & \dots & 0 \\ 0 & 1 & 0 & \dots & 0 \\ \vdots & \vdots & \ddots & \vdots & \vdots \\ 0 & \dots & 0 & 1 & 0 \\ 0 & \dots & 0 & 0 & -r \end{bmatrix}. \tag{6}$$

We assume that the damping matrix $[C]$ is linearly proportional to the stiffness matrix $[K]$, such that equation 4 can be decoupled for a set of $[M], [C], [K]$ matrices in the usual way (Meirovitch 1967). We consider the simplest case where $m_j = m$, $c_j = c$, $k_j = k$ for $j = 1, 2, \dots, N$. This assumption is analogous to a commonly used modelling technique, where systems with continuous, uniformly distributed mass and stiffness, are assumed instead to consist of a series of lumped masses. Thus we can rewrite Eq. (4) in the form

$$[I]\ddot{\mathbf{x}} + \frac{c}{m}[E]\dot{\mathbf{x}} + \frac{k}{m}[E]\mathbf{x} = \frac{1}{m}\mathbf{f}(t) \tag{7}$$

where $[E]$ is the $N \times N$ coupling matrix

$$[E] = \begin{bmatrix} 2 & -1 & 0 & 0 & \dots & 0 \\ -1 & 2 & -1 & 0 & \dots & 0 \\ 0 & -1 & 2 & -1 & \dots & 0 \\ \vdots & \dots & \ddots & \ddots & \dots & \vdots \\ 0 & \dots & -1 & 2 & -1 & 0 \\ 0 & \dots & 0 & -1 & 2 & -1 \\ 0 & \dots & 0 & 0 & -1 & 1 \end{bmatrix}, \tag{8}$$

and $[I]$ is the identity matrix.

2.1 Modal decoupling

Away from impact, $x_N < x_s$ the system is governed by Eq. (7). By considering the undamped, unforced, (non-impacting) system, the natural frequencies of the system are given by $\omega_j = \sqrt{\lambda_j k/m}$ for $j = 1, 2, \dots, N$ (Timoshenko *et al.* 1974) where λ_j are the eigenvalues of matrix $[E]$. The eigenvectors ξ_j corresponding to each λ_j normalised such that $\| \xi_j \| = 1$ define the corresponding mode shapes of the system. Using these eigenvectors we can construct a modal matrix $[\Psi] = [\{\xi_1\}, \{\xi_2\}, \dots, \{\xi_N\}]$. The modal matrix is orthogonal such that $[\Psi]^T = [\Psi]^{-1}$. In addition $[\Psi]^T[E][\Psi] = [\Lambda]$, the diagonal matrix of the eigenvalues of $[E]$.

We can then define modal coordinates, using the linear transform $\mathbf{x} = [\Psi]\mathbf{q}$ where $\mathbf{q} = \{q_1, q_2, \ldots q_N\}^T$. Substituting this into Eq. (7) and premultiplying by $[\Psi]^T$ decouples the system to give

$$[I]\ddot{\mathbf{q}} + \frac{c}{m}[\Lambda]\dot{\mathbf{q}} + \frac{k}{m}[\Lambda]\mathbf{q} = \frac{1}{m}[\Psi]^T\mathbf{f}(t). \tag{9}$$

Equation (9) represents a set of N uncoupled equations such that for each mode of vibration

$$\ddot{q_j} + 2\zeta_j\omega_j\dot{q_j} + \omega_j^2 q = \frac{1}{m}\sum_{i=1}^{N}\Psi_{ij}^T f_i, \quad j = 1, 2, \ldots, N, \tag{10}$$

where $\zeta_j = (c/2)\sqrt{\lambda_j/km}$ is the modal damping coefficient. Hence in modal coordinates the effect of the forcing is distributed across each mode via the modal matrix Ψ^T such that each mode is separately subjected to a proportion of the overall forcing terms.

However, the motion of the system is constrained such that $x_N < x_s$ during free flight of mass N. If we define the vector $\psi = \{\Psi_{N1}, \Psi_{N2}, \ldots, \Psi_{NN}\}^T$, then in terms of modal coordinates an impact occurs when $\psi \cdot \mathbf{q} = x_s$. Hence Eqs. (9) and (10) are valid only for $\psi \cdot \mathbf{q} < x_s$ which is equivalent to the condition that $x_N < x_s$.

We will consider only harmonic forcing of the form $\mathbf{f}(t) = \mathbf{A}\cos(\Omega t)$, $\mathbf{A} = \{A_1, A_2, \ldots, A_N\}^T$. Thus we can simplify Eq. (10) to give

$$\ddot{q_j} + 2\zeta_j\omega_j\dot{q_j} + \omega_j^2 q = \frac{F_j}{m}\cos(\Omega t), \tag{11}$$

where $\mathbf{F} = [\Psi]^T\mathbf{A}$, $\mathbf{F} = \{F_1, F_2, \ldots, F_N\}^T$.

Equation (11) can be solved exactly, and for under-damped oscillations $0 < \zeta_j < 1$ the solution for the jth mode is

$$q_j = e^{-\zeta_j\omega_j(t-t_0)}(B_i\cos(\omega_{dj}(t-t_0)) + C_i\sin(\omega_{dj}(t-t_0))) + Q_j\cos(\Omega t - \phi_j) \tag{12}$$

where $\omega_{dj} = \omega_j\sqrt{1-\zeta_j^2}$ is the damped natural frequency. Also

$$Q_j = \frac{F_i}{m\left[(\omega_j^2 - \Omega^2)^2 + (2\zeta_j\Omega\omega_j)^2\right]^{1/2}} \tag{13}$$

is the jth modal transfer function,

$$\phi_j = \arctan\left(\frac{2\zeta_j\Omega\omega_j}{(\omega_j^2 - \Omega^2)}\right) \tag{14}$$

is the jth modal phase and B_i and C_i are arbitrary constants determined from the initial conditions.

2.2 Initial conditions and computing solutions

Away from or between impacts $x_N < x_s$, we can find the exact solution for any N degree of freedom system with constant mass, stiffness and viscous damping. We therefore take initial conditions just after an impact such that $t_0 = t_+$. Initial conditions for each modal displacement and velocity can then be found using the relation $\mathbf{q} = [\Psi]^{-1}\mathbf{x}$ and the time derivative $\dot{\mathbf{q}}$. In general the time of impact cannot be found analytically (Shaw & Holmes 1983), and as a result solutions must still be computed numerically. This is achieved by iterating the exact solution, Eq. (12), forward in small time increments Δt until an impact has occurred, then a root finding method is used to locate the time of impact. The impact rule, Eq. (5), is then applied before the next iteration. Thus, by computing the evolution of the modal trajectories between impacts, we are in effect computing the impact map for the system.

As, in this formulation, only a single mass is constrained, this map can be defined in a similar way to the map for a single degree of freedom system (Shaw & Holmes 1983). The impact map is formed by considering the hypersurface in phase space, Σ, defined by the impact stop $x_N = x_s$. This is a Poincaré type section through the flow, in phase space $\mathcal{R}^n$, where for a N degree of freedom oscillator $n = 2N + 1$, for example, a two degree of freedom system has a five dimensional phase space. The impact map is formed by intersections between this section and the flow. For systems with a single impacting mass we can project the dynamics of the impact map into two dimensional plane, defined by impact velocity and time (or phase; time modulo the forcing frequency) of the impacting mass. Conceptually this allows us to view the effect of higher dimensional dynamics on an impacting system, reduced to an impact map of the same dimension as that for a single degree of freedom system.

Periodic orbits in the flow, can be locate as fixed points in the impact map $P_I : (\tau_i, v_i)_j \mapsto (\tau_i, v_i)_{j+1}$, where v_i represents the velocity of mass N at impact, and τ_i the corresponding time of impact. Thus for a fixed point $\eta = \{\tau_i, v_i\}$, $\eta \in \Sigma$, of the map P_I, $P_I(\eta) - \eta = 0$. Defining the residual map $U(\eta) = P_I(\eta) - \eta$, a fixed point corresponds to $U(\eta) = 0$. The fixed points can be computed using the Newton-Raphson root finding method as described by Foale & Thompson (1991). To implement this procedure numerically, we have to include all variables of the linear system except x_N which is always equal to x_s in the impact map. Thus we form a vector $\eta = \{x_1, \ldots, x_{N-1}, \tau_i, v1, \ldots, v_i\}$ for this purpose, where τ_i, the time of impact of mass N, is used as a variable instead of x_N.

For the single degree of freedom system it is possible to obtain analytical expressions for

eigenvalues, (Shaw & Holmes 1983), but for systems with more than a single degree of freedom such expressions are not readily available. Pun *et al.* (1998) used a variational type method to compute stability for a two degree of freedom system. This requires some analytical and computational effort, especially for systems with $N > 2$. For this analysis, we have instead used a finite difference approximation detailed in Foale & Thompson (1991). Thus, when a fixed point in the impact map has been found using the Newton-Raphson method, it's stability can be determined by examining the eigenvalues of the Jacobian of the impact map. Finally by extending the variable space to include a parameter μ, such that $\eta = \{x_1, \ldots, x_{N-1}, \tau_i, v1, \ldots, v_i, \mu\}$, we can follow the path of a fixed point solution as μ is varied.

A significant drawback of these path following methods is that they fail to work when non-smooth discontinuities are present in the dynamics of the system. This occurs in impacting systems at a grazing bifurcation (Nordmark 1991). Thus for the numerical simulations in section 3, we use the path following methods only for locally identifying bifurcations of fixed points.

3 Example: A two degree of freedom system

As an example, we consider a two degree of freedom impact oscillator with, masses $m_1 = m_2 = 1$, stiffness $k_1 = k_2 = 1$, viscous damping $c_1 = c_2 = 0.1$, coefficient of restitution $r = 0.7$ and stop distance $x_s = 0.1$. This parameter choice will enable us to investigate a wide range of dynamical behaviour including chaos, chatter and sticking. The choice of $c = 0.1$ and $r = 0.7$ is in relevant to the energy loss characteristics of a wide range of mechanical systems. By selecting the stop distance $x_s = 0.1$ impacting motion can occur for a wide frequency range, but the system is also capable of non-impacting motion. Finally we choose unity mass and stiffness values to obtain a simplified relationship between the natural frequency values and the system eigenvalues.

Using Eqs. (1) and (2), the equations of motion for the coupled masses can be expressed as

$$\begin{aligned} \ddot{x}_1 + 0.1(2\dot{x}_1 - \dot{x}_2) + (2x_1 - x_2) &= f_1(t), \\ \ddot{x}_2 + 0.1(\dot{x}_2 - \dot{x}_1) + (x_2 - x_1) &= f_2(t). \end{aligned} \tag{15}$$

where x_1 represents the displacement of mass m_1 and x_2 the displacement of mass m_2. When $x_2 = x_s$ an impact occurs and an instantaneous coefficient of restitution rule is applied via Eq. (3), such that $\dot{x}_2(t_+) = -0.7\dot{x}_2(t_-)$.

Setting $A_2 = 0$ and $A_1 = 0.5$, the *non-impacting* response of the system is shown in Fig. 2. This

shows a numerically generated plot of the maximum minus the minimum displacement per period for each mass against forcing frequency Ω. The solid line corresponds to the displacement of x_2 and the broken line to the displacement of x_1. Two clear resonance peaks can be seen corresponding to the two natural frequencies of the non-impacting system, $\omega_1 = 0.618$ and $\omega_2 = 1.618$.

The eigenvalues of the 2×2 coupling matrix $[E]$ are $\lambda_1 = 0.382$ and $\lambda_2 = 2.618$, and the corresponding normalised eigenvectors, $\xi_1 = [0.526, 0.851]^T$ and $\xi_2 = [-0.851, 0.526]^T$, give the mode shapes for the system. We see that for mode 1 the masses are in phase, and mode 2 the masses are out of phase (Timoshenko *et al.* 1974).

3.1 Vibro-impact motions

A bifurcation diagram indicating the maximum minus minimum displacement (x_2) of mass 2 sampled per period of forcing for the two degree of freedom example, is shown in Fig. 3 (a). Regimes of both periodic and non-periodic impacting motion exist within this parameter range, and we classify periodic impacting motions as $\mathbf{P}(p, q)$, where p impacts occur in q forcing periods of $2\pi/\Omega$. For the periodic regimes, Fig. 3 (a) indicates periodicity of the motion in terms of the number of forcing periods q.

In Fig. 3 (b) the velocity at impact $v_i = \dot{x}_2(t_-)$ is plotted against forcing frequency. This figure indicates the periodicity of the motion in terms of the number of impacts p. By comparing the two figures we can see for example, that at $\Omega = 0.6$ a $\mathbf{P}(2, 1)$ solution exists; two impacts ($p = 2$) from Fig. 3 (b) in one forcing period ($q = 1$) from Fig. 3 (a). The time series of this motion is shown in Fig. 4 (d), where the displacement x_1 is shown as a broken line, x_2 as a solid line and the position of the impact stop, x_s, corresponds to 0.1 on the displacement axis.

Increasing Ω, the $\mathbf{P}(2, 1)$ solution undergoes a series of bifurcations at $\Omega \approx 0.85$ after which it stabilises onto a $\mathbf{P}(1, 1)$ solution. The time series for this $\mathbf{P}(1, 1)$ solution is shown in Fig. 4 (e) where $\Omega = 0.9$. At $\Omega = 1.4$ the solution is still $\mathbf{P}(1, 1)$, Fig. 4 (f), but the oscillation of x_1 is now reduced and offset from the origin. The $\mathbf{P}(1, 1)$ solution bifurcates into a $\mathbf{P}(2, 2)$ solution via a period doubling bifurcation at $\Omega \approx 1.61$, and again at $\Omega \approx 1.68$ such that at $\Omega = 1.7$ a $\mathbf{P}(4, 4)$ solution exists, Fig. 4 (g). After this the motion becomes chaotic with a small window of $\mathbf{P}(2, 3)$ motion at $\Omega \approx 1.74$.

Again increasing Ω the motion becomes stable as a $\mathbf{P}(1, 2)$ impacting motion, Fig. 4 (h). At $\Omega \approx 2.19$ the motion becomes non-impacting. The impact map is undefined for this motion as can be seen in Fig. 3 (b).

3.2 Grazing bifurcation leading to changes in periodicity

Considering more carefully the bifurcations which occur between vibro-impact motions, we examine the region close to $\Omega = 0.85$. Figure 5 (a) shows a close up of the bifurcation diagram near $\Omega = 0.85$. In this figure dots correspond to the numerically computed solution, and the line shown in the right hand side of the figure was computed using the path following method outlined in Sec. 2.2, by decreasing Ω from $\Omega = 1.0$. This computation breaks down at a bifurcation point close to $\Omega = 0.856$, as additional impacts occur, destroying the $\mathbf{P}(1,1)$ fixed point in the impact map.

We can understand the behaviour of this region by considering the time series plots shown in Fig. 5 (b), (c) and (d). Figure 5 (b) shows the $\mathbf{P}(2,1)$ motion which exists at $\Omega = 0.83$. At $\Omega \approx 0.831$ the motion "loses" an impact via a grazing bifurcation. However, instead of becoming a $\mathbf{P}(1,1)$, the period of the motion doubles such that a $\mathbf{P}(3,2)$ motion is formed, Fig. 5 (c). In fact from Fig. 5 (c) we see that the first period of the $\mathbf{P}(3,2)$ motion (between the first and third impacts) is qualitatively similar to the $\mathbf{P}(2,1)$ motion, only in the second period (between the third and fourth impact) can the loss of an impact be seen. Thus in this case the periodicity of the motion has changed in an apparently additive way $\mathbf{P}(p,q) \mapsto \mathbf{P}(p+1, q+1)$, although the underlining cause of the bifurcation is the grazing event which occurs close to $\Omega = 0.831$.

Increasing Ω, the $\mathbf{P}(3,2)$ motion persists, until another bifurcation occurs at $\Omega \approx 0.856$. Again the underling cause of this change in behaviour is due to a grazing event. The motion loses an impact, and the period of the motion halves simultaneously, such that a $\mathbf{P}(1,1)$ motion occurs, Fig. 5 (d). By comparing Fig. 5 (c) and (d), we observe that in effect the first period of the $\mathbf{P}(3,2)$ motion has lost an impact, such that the two period are now the same and the periodicity of the motion thus halves.

These bifurcations are interesting because changes of periodicity and number of impacts change simultaneously, in an apparently non-symmetric way. The cause of this behaviour in the two degree of freedom system, is due primarily to the occurrence of a grazing bifurcation which occurs when Ω is altered. This grazing bifurcation leads to a period of transient instability after which the system is attracted to a new (in this case periodic) solution. We conjecture from our simulations that during the period of transient instability directly after grazing, the influence of the additional mass in the system is significant. As a result we observe periodic solutions which we would not normally observe in a single degree of freedom system.

For this particular set of parameter values no saddle node type bifurcations were observed, and

no regions of hysteresis have been shown to exist. This again is in contrast to the single degree of freedom system impact oscillator, where hardening spring behaviour is observed.

3.3 Resonance Peaks

An interesting feature of the bifurcation diagram shown in Fig. 3 (a) is the occurrence of three clear resonance peaks at forcing frequency values of $\Omega \approx 0.82$, $\Omega \approx 1.17$ and $\Omega \approx 1.69$. Comparing this with Fig. 3 (b) for the impact velocity a clear resonance peak can be seen at $\Omega \approx 1.16$ with lesser peaks at $\Omega \approx 0.82$ and $\Omega \approx 1.69$. This implies that at $\Omega \approx 0.82$ and $\Omega \approx 1.69$ the impact velocities are less than the main resonance peak but that the difference between the maximum and minimum displacement per period is almost the same as the main resonance peak.

This effect is due to the difference in the vibro-impact motions at each resonance peak. When $\Omega \approx 0.82$ the motion is $\mathbf{P}(2,1)$, at $\Omega \approx 1.17$ the motion is $\mathbf{P}(1,1)$, and at $\Omega \approx 1.69$ the motion becomes $\mathbf{P}(4,4)$. Figure 6 shows the phase portrait of each of these motions, from which it can be seen how the maximum displacement of each motion is approximately the same but the impact velocity of the $\mathbf{P}(1,1)$ motion (Fig. 6 (b)) is significantly greater than the impact velocities of the other two motions.

We also note that the occurrence of these resonance peaks does not coincide with the non-impacting resonance peaks on the frequency axis. This is not unexpected for an impact oscillator, as it is known for a single degree of freedom system that reducing the stop distance increases the resonant frequency of the system (Todd & Virgin 1996). This analysis is based on a $\mathbf{P}(1,1)$ motion, and for a stop distance of zero the resonant frequency of the single degree of freedom impact oscillator is double that of the non-impacting oscillator.

This could account for the resonance peak around $\Omega \approx 1.17$ which is close to double the first natural frequency of the system, and the motion is $\mathbf{P}(1,1)$. In fact considering only Fig. 3 (b), where the main resonance occurs at this value, this would seem appropriate. However, there is no similar peak corresponding to a value double that of the second natural frequency. Thus for the two degree of freedom system, the increase in natural frequency appears similar to that which occurs in the single degree of freedom system occurs for $\mathbf{P}(1,1)$ motion only. The resonant behaviour which occurs at $\Omega \approx 0.82$ and $\Omega \approx 1.69$, is a result of different periodic impacting motions, and cannot be predicted by our knowledge of single degree of freedom system dynamics.

3.4 Sticking and chatter motions

For chattering to occur in a vibro-impact system, the acceleration of the impacting mass must remain positive for a sequence of low velocity impacts. If the sequence is long enough the velocity of the impacting mass tends to zero such that the mass effectively becomes stuck to the stop. Chatter leading to sticking is referred to as complete chatter, if the sequence does not lead to sticking the chatter is incomplete. A detailed study of this behaviour including the dynamics associated with such motions in the single degree of freedom impact oscillator has been considered by Budd & Dux (1994a).

After a complete chatter sequence, the impacting mass, m_2 for the two degree of freedom system, is held against the stop. The force holding m_2 in this position during sticking is given by

$$F_s = c\dot{x}_1 + k(x_1 - x_s). \tag{16}$$

Thus the mass will remain against the stop while $F_s > 0$, and the point where F_s decreases through zero represents the end of the sticking motion.

While m_2 is stuck to the stop, only m_1 can oscillate. The motion of m_1 is then governed by the equation

$$\ddot{x}_1 + 2(0.1)\dot{x}_1 + (2x_1 - x_2) = 0.5\cos(\Omega t). \tag{17}$$

When trying to model the system numerically, a chattering sequence leads to the time between impacts decreasing rapidly to zero. In order to overcome the resulting computational difficulties, we adopt the method proposed by Cusumano & Bai (1993) by setting a threshold level for the interval between impacts. Once the time interval between impacts falls below this level we assume m_2 is stuck to the stop. The time at which $F_s = 0$ is computed by root finding to locate the end of the sticking period. We note that the method of Cusumano & Bai (1993) may have limitations for certain systems (Johansson *et al.* 1999; Johansson *et al.* 1999).

Impacting motion occurs in the range $0 < \Omega < 2.19$. For higher Ω values, the period decreases such that chattering remains incomplete. In fact for this set of parameters all sticking motions (i.e. complete chatter) are observed for $\Omega < 0.35$. This can be seen in Fig. 3 (b) where sticking motions exist in the range $0.2 < \Omega < 0.35$. In addition for $\Omega > 0.35$, impact velocities become much higher, so that motions become periodic impacting motions with a high number of impacts q rather than incomplete chatter motions. This said, defining the boundary between these two types of motion is difficult. For example Fig. 4 (c) shows the time series of the motion just after the

region of sticking motions at $\Omega = 0.4$, which is $\mathbf{P}(4, 1)$. Thus for this model, chatter and sticking motions occur in regions of low forcing frequency where the response has low amplitude.

Examples of a periodic motion with both chatter and sticking are shown in Fig. 4 (a) and (b). As there are effectively an infinite number of impacts during the period (under the assumption of an instantaneous impact rule) we denote such a motion as $\mathbf{P}(\infty, q)$. Considering Fig. 4 (b) during one period, starting at time $t = 770$ for example, the motion of mass 2 is in free flight and approximately in phase with the motion of mass 1. At time $t \approx 778$ a first impact occurs, followed by a complete chatter sequence until mass 2 becomes stuck to the stop. During this time mass 1 is displaced beyond the stop distance thus causing F_s to remain positive. As mass 1 returns from beyond the stop, F_s passes through zero and m_2 is thus released from the sticking position into free flight again. The period of the forcing is approximately 31.42 seconds, thus we can see that the motion repeats in one period of forcing, i.e. from $t = 770$ to $t \approx 801.42$ seconds. Therefore the motion can be characterised as $\mathbf{P}(\infty, 1)$ motion. It is interesting to note that during the time when mass 2 is chattering and then sticking, mass 1 appears to have an additional higher frequency oscillation. This effect can be seen more clearly in Fig. 4 (a) where $\Omega = 0.1$.

A close up of the sticking region of the bifurcation diagram, Fig. 3 (b), is shown in Fig. 7. This includes the motions shown in Fig. 4 (a) and (b). At a forcing frequency of $\Omega = 0.2$ the complete chatter combined with sticking motion exists. As the forcing frequency is increased this type of motion persists until a frequency just greater than $\Omega = 0.3$. At this value the sticking phase of motion no longer exists, so the chatter is incomplete. Continuing to increase frequency this motion successively losses impacts until the $\mathbf{P}(2, 1)$ motion is reached at $\Omega \approx 0.47$.

The sticking region itself appears to have a complex bifurcation structure. There are two points $\Omega \approx 0.138$ and $\Omega \approx 0.228$ where the impact velocities of the chatter sequence becomes small compared to the rest of the region. Between these points chattering sequences with higher impact velocities are encountered, although in comparison with the complete bifurcation diagram 3 (b) all the impact velocities for chatter and sticking motions are all relatively low.

3.5 Chaotic motion

For the set of parameters used in this example, the two degree of freedom system exhibits a range of chaotic motion between $\Omega = 1.7$ and $\Omega = 1.82$. We have computed the impact map for the two degree of freedom system for a set of Ω values across this chaotic range, Fig. 8. Here we can see the initial transition from $P(4, 4)$ impacting motion at $\Omega \approx 1.71$ to chaotic motion as Ω is

increased. Continuing to increase Ω, the motion again becomes $P(4,4)$ at $\Omega \approx 1.725$, then $P(2,2)$ and back to chaotic motion at $\Omega \approx 1.75$. Finally the motion changes from chaotic to $P(2,2)$ at $\Omega \approx 1.81$.

The changes in the structure of the chaotic attractors can be clearly seen as Ω is varied. Four of these chaotic attractors $\Omega \approx 1.701, 1.72, 1.75, 1.81$ occur at an Ω value close to a grazing bifurcation from periodic motion. These are the attractors of primary interest in this study, as they relate to the parameter values for which a low dimensional mapping which approximates the dynamics of the system, may be possible. Qualitatively, it appears that the attractors close to grazing are composed (at least in part) of a series of disconnected one dimensional sets. This can be seen clearly in the attractor when $\Omega = 1.72$, which appears to be composed of two disconnected one dimensional sets, one containing "low" velocity impacts, and the other "high" velocity impacts. A close up of the "high" velocity set is shown in Fig. 9 (c), where the (approximately) one dimensional nature can be clearly seen. Also evident from this figure is a sharp point of discontinuity in the set, a characteristic feature of impact systems, close to grazing.

The attractor which occurs when $\Omega = 1.701$ does not divide simply into attracting regions of "high" and "low" velocity impacts, here there appears to be a set containing "medium" velocity impacts as well. The structure of this "medium" set is shown in detail in Fig. 9 (a). This complex structure appears qualitatively, to be composed of many one dimensional sets. However, unlike in the single degree of freedom system, a "fingered" structure is not evident. However, finger like structures are visible in the high velocity set when $\Omega = 1.701$, as well as in the attractors which occur at $\Omega = 1.75$ and $\Omega = 1.77$.

Away from grazing, the structure of the attractors have less one dimensional components. A close up of the region of high velocity impacts found when $\Omega = 1.715$ is shown in Fig. 9 (b). This structure appears to be similar to the "spiral" structures observed in the work on DC/DC Buck converters by di Benardo *et al.* (1998). Although, unlike the spirals in the Buck converter, those in our study have nonsmooth points at one end only, Fig. 9 (b).

3.5.1 Low dimensional mappings

For single degree of freedom impact oscillators close to a grazing bifurcation, the corresponding chaotic attractors have been shown to be composed of a series of one dimensional sets (Budd & Dux 1994b). This has led to the development of a one dimensional mapping which represents the underlying dynamics of a single degree of freedom system close to grazing (Nordmark 1997). This

map can be expressed as

$$X_{n+1} = \begin{cases} s\sqrt{d - X_n} + \lambda X_n & X_n \leq d \\ \lambda X_n & X_n > d \end{cases} \tag{18}$$

where now d is the bifurcation parameter and s and λ are constant parameters, usually scaling allows us to take $s = 1$. An example of the functional form of this map is shown in figure 11 when $d = s = 1$ and $\lambda = 0.2$. Fredriksson & Nordmark (1997) investigated the possibility of extending this mapping concept to impact oscillators with many degrees of freedom, and found that an approximate local mapping of low (close to one) dimension could be formulated.

Budd & Dux (1994b) tested for the possible existence of a one dimensional map by plotting a return map $v_i(j) \rightarrow v_i(j+1)$, of low velocity impacts, from which they found a discontinuous, but approximately one dimensional relationship existed close to grazing. The return map of low velocity impacts ($v_i < 0.3$) for the 'low' velocity set when $\Omega = 1.72$ is shown for the two degree of freedom system system in Fig. 10 (a). Here we can see that the relationship between successive low velocity impacts is approximately one dimensional (and branched) except in the range $0.22 < v_i(j) < 0.23$, where more complex dynamics exist. In fact this structure appears to have qualitative similarities with the one dimensional map developed for the the single degree of freedom impact oscillator, Eq. 18 (Fig. 11). The one dimensional mapping is the composition of a linear (straight line) part and a parabolic part, which are joined at $Xn = d$ by a nonsmooth discontinuity. The structure in Fig. 10 (a) also has an approximately linear part, and a parabolic curved structure, although there is no evident nonsmooth discontinuity. This provides numerical evidence for the existence of low dimensional mappings in N degree of freedom oscillators as suggested by (Fredriksson & Nordmark 1997).

For other attractors close to grazing more complex dynamics appear to predominate. For example, the return mapping of low velocity impacts ($v_i < 0.22$) for the attractor which exists when $\Omega = 1.75$ is shown in Fig. 10 (b). Here, there is no evident one dimensional relationship between successive low velocity impacts, despite the appearance of one dimensional sets in the original attracting structure, Fig. 8. In fact, the attractor at $\Omega = 1.72$ is the only one for this example which has a close to one dimensional relationship between successive low velocity impacts. In which case the formulation of a low dimensional mapping may only be possible for this grazing event alone.

A further observation regarding the attractor at $\Omega = 1.72$, is that it's low velocity set is bounded from above and below, such that $0.15 < v_i < 0.25$. This is in contrast to all the other attractors,

where the low velocity set has impact velocities which tend to zero, $v_i \to 0$.

3.5.2 Chaotic chatter

Finally, we note one further point regarding this region of chaotic motion. The transition between periodic and chaotic motion will typically occur via grazing or period doubling. However, in the region between the chaotic attractor at $\Omega = 1.72$ and the $\mathbf{P}(4, 4)$ motion at $\Omega = 1.725$, a region of *chaotic chatter* exists. A typical time series of this motion is shown in Fig. 12. This motion occurs after a $\mathbf{P}(32, 32)$ motion, but just before the more regular chaotic motion at $\Omega = 1.72$.

4 Conclusions

In this work we have considered the dynamics of multi-degree of freedom impact oscillators, using the example of a two degree of freedom system. From a detailed numerical study of this system we have observed a range of dynamical behaviour, including periodic motion, chatter (both periodic and chaotic), sticking and chaos. Of particular interest are phenomena which do not occur in single degree of freedom system, such as non-symmetric changes in periodicity, multiple resonance peaks and the existence of chatter in a system without preloading. From a modelling perspective, if such phenomena occur in a physical system, then using a multi-degree of freedom model may be necessary to capture the dynamics of the system.

We have also studied the nature of the chaotic motion which can occur for the two degree of freedom example. We observed that for a set parameter values where the system is close to grazing, it may be possible to formulate a low dimensional relationship between low velocity impacts. This is concurrent with the work carried out by Fredriksson & Nordmark (1997) who reduced the dynamics of a multi-degree of freedom impact oscillator (locally close to grazing) to a nearly one dimensional map. However, this is a highly localised phenomena in the system studied here, which itself is only one set of parameter values from a much wider range. At other grazing events more complex dynamics occur for which low dimensional mappings would not be applicable.

References

Bishop, R. E. D. & Johnson, D. C. (1960). *The mechanics of vibration*. Cambridge University Press.

Budd, C. J. & Dux, F. (1994a). Chattering and related behaviour in impact oscillators. *Philosophical Transactions of the Royal Society of London A* **347**, 365–389.

Budd, C. J. & Dux, F. (1994b). Intermittency in impact oscillators close to resonance. *Nonlinearity* **7**, 1191–1224.

Chatterjee, S., Mallik, A. K. & Ghosh, A. (1995). On impact dampers for non-linear vibrating systems. *Journal of Sound and Vibration* **187**(3), 403–420.

Cusumano, J. P. & Bai, B-Y. (1993). Period-infinity periodic motions, chaos and spatial coherence in a 10 degree of freedom impact oscillator. *Chaos, Solitons and Fractals* **3**, 515–536.

di Benardo, M., Champneys, A. R. & Budd, C. J. (1998). Grazing, skipping and sliding: analysis of the non-smooth dynamics of the DC/DC buck converter. *Nonlinearity* **11**(4), 858–890.

Foale, S. & Thompson, J. M. T. (1991). Geometrical concepts and computational techniques of nonlinear dynamics. *Computer Methods For Applications In Mechanical Engineering* **89**, 381–394.

Fredriksson, M. H. & Nordmark, A. B. (1997). Bifurcations caused by grazing incidence in many degrees of freedom impact oscillators. *Proceedings of the Royal Society of London A* **453**, 1261–1276.

Gladwell, G. M. L. (1986). *Inverse problems in vibration*. Dordrecht: Kluwer.

Johansson, K. H., Egerstedt, M., Lygeros, J. & Sastry, S. (1999). On the regularization of Zeno hybrid automata. *System and Control Letters* **38**, 141–150.

Johansson, K. H., Lygeros, J., Sastry, S. & Egerstedt, M. (1999). Simulation of Zeno hybrid automata. In *Proceedings of IEEE Conference on Desision and Control*, Phoenix, Arizonia, USA.

Masri, S. F. (1972). Theory of the dynamic vibration neutraliser with motion-limiting stops. *Transactions of the American Society of Mechanical Engineers, Journal of Applied Mechanics* **39**, 563–568.

Meirovitch, L. (1967). *Analytical methods in vibration*. New York: McGraw-Hill.

Natsiavas, S. (1993). Dynamics of multiple-degree-of-freedom oscillators with colliding components. *Journal of Sound and Vibration* **165**(3), 439–453.

Neilson, R. D. & Gonsalves, D. H. (1993). Chaotic motion of a rotor system with a bearing clearance. In *Applications of fractals and chaos*, A. J. Crilly, R. A. Earnshaw, & H. Jones (Eds.), 285–303. Springer-Verlag.

Nigm, M. M. & Shabana, A. A. (1983). Effect of an impact damper on a multi-degree of freedom system. *Journal of Sound and Vibration* **89**(4), 541–557.

Nordmark, A. B. (1991). Non-periodic motion caused by grazing incidence in an impact oscillator. *Journal Of Sound and Vibration* **145**(2), 275–297.

Nordmark, A. B. (1997). Universal limit mapping in grazing bifurcations. *Physical Review E* **55**, 266–270.

Pun, D., Lua, S. L., Law, S. S. & Cao, D. Q. (1998). Forced vibration of a multidegree impact oscillator. *Journal of Sound and Vibration* **213**(3), 447–466.

Shaw, J. & Shaw, S. W. (1989). The onset of chaos in a two-degree of freedom impacting system. *Journal of Applied Mechanics* **56**, 168–174.

Shaw, S. W. & Holmes, P. J. (1983). A periodically forced piecewise linear oscillator. *Journal of Sound and Vibration* **90**(1), 129–155.

Timoshenko, S. P., Young, D.H. & Weaver Jr, W. (1974). *Vibration problems in engineering.* Van Nostrand USA.

Todd, M. D. & Virgin, L. N. (1996). Natural frequency considerations of an impact oscillator. *Journal of Sound and Vibration* **194**(3), 452–460.

International Journal of Bifurcation and Chaos, Vol. 11, No. 1 (2001) 57–71

Figure Captions

- Figure 1. Schematic representation of an N degree of freedom impact oscillator.

- Figure 2. Numerically computed non-impacting resonance curves for the two degree of freedom coupled linear oscillator, maximum minus minimum displacement *vs* forcing frequency. Parameter values $m_1 = m_2 = 1$, $k_1 = k_2 = 1$, $c_1 = c_2 = 0.1$, forcing $A_2 = 0.0$, $A_1 = 0.5$. Solid line represents x_2, dotted line represents x_1.

- Figure 3. Numerically computed two degree of freedom impact oscillator bifurcation diagram. Parameter values $m_1 = m_2 = 1$, $k_1 = k_2 = 1$, $c_1 = c_2 = 0.1$, $x_s = 0.1$, $r = 0.7$, forcing $A_2 = 0.0$, $A_1 = 0.5$. (a) maximum minus minimum displacement x_2 per period *vs* forcing frequency Ω. (b) Impact velocity $\dot{x}_2(t_-)$ *vs* forcing frequency Ω.

- Figure 4. Numerically computed time series for a two degree of freedom impact oscillator. Solid line x_2, broken line x_1. Parameter values $m_1 = m_2 = 1$, $k_1 = k_2 = 1$, $c_1 = c_2 = 0.1$, $x_s = 0.1$, $r = 0.7$, forcing $A_2 = 0.0$, $A_1 = 0.5$. (a) $\Omega = 0.1$ (b) $\Omega = 0.2$; (c) $\Omega = 0.4$; (d) $\Omega = 0.6$ (e) $\Omega = 0.9$; (f) $\Omega = 1.4$; (g) $\Omega = 1.7$; (h) $\Omega = 2.0$.

- Figure 5. Identifying bifurcations for two degree of freedom impact oscillator example shown in Fig. 3. (a) close up of bifurcation diagram: Time series of motion; (b) $\Omega = 0.83$; (c) $\Omega = 0.85$; (d) $\Omega = 0.87$.

- Figure 6. Numerically computed two degree of freedom impact oscillator phase portrait showing large amplitude motions. Solid line x_2, broken line x_1. Parameter values; $m_1 = m_2 = 1$, $k_1 = k_2 = 1$, $c_1 = c_2 = 0.1$, $A_1 = 0.5$, $A_2 = 0.0$, $x_s = 0.1$, $r = 0.7$ and $r = 0.7$. (a) $\Omega = 0.82$; (b) $\Omega = 1.17$; (c) $\Omega = 1.69$.

- Figure 7. Two degree of freedom impact oscillator numerical bifurcation diagram; chatter and sticking region. Parameter values $m_1 = m_2 = 1$, $k_1 = k_2 = 1$, $c_1 = c_2 = 0.1$ forcing $A_2 = 0.0$, $A_1 = 0.5$, $x_s = 0.1$ and $r = 0.7$.

- Figure 8. Numerically computed impact maps for a two degree of freedom impact oscillator. Parameter values $m_1 = m_2 = 1$, $k_1 = k_2 = 1$, $c_1 = c_2 = 0.1$, $x_s = 0.1$, $r = 0.7$, forcing $A_2 = 0.0$, $A_1 = 0.5$.

- Figure 9. Features of the numerically computed impact maps for a two degree of freedom impact oscillator. Parameter values $m_1 = m_2 = 1$, $k_1 = k_2 = 1$, $c_1 = c_2 = 0.1$, $x_s = 0.1$, $r = 0.7$, forcing $A_2 = 0.0$, $A_1 = 0.5$.

- Figure 10. Numerically computed Impact velocity return maps for a two degree of freedom impact oscillator. Parameter values $m_1 = m_2 = 1$, $k_1 = k_2 = 1$, $c_1 = c_2 = 0.1$, $x_s = 0.1$, $r = 0.7$, forcing $A_2 = 0.0$, $A_1 = 0.5$.

- Figure 11. Functional form of the one dimensional impact map for $s = d = 1$ and $\lambda = 0.2$.

- Figure 12. Chaotic chatter motion.Parameter values $m_1 = m_2 = 1$, $k_1 = k_2 = 1$, $c_1 = c_2 = 0.1$, $x_s = 0.1$, $r = 0.7$, forcing $A_2 = 0.0$, $A_1 = 0.5$, $\Omega = 1.721$.

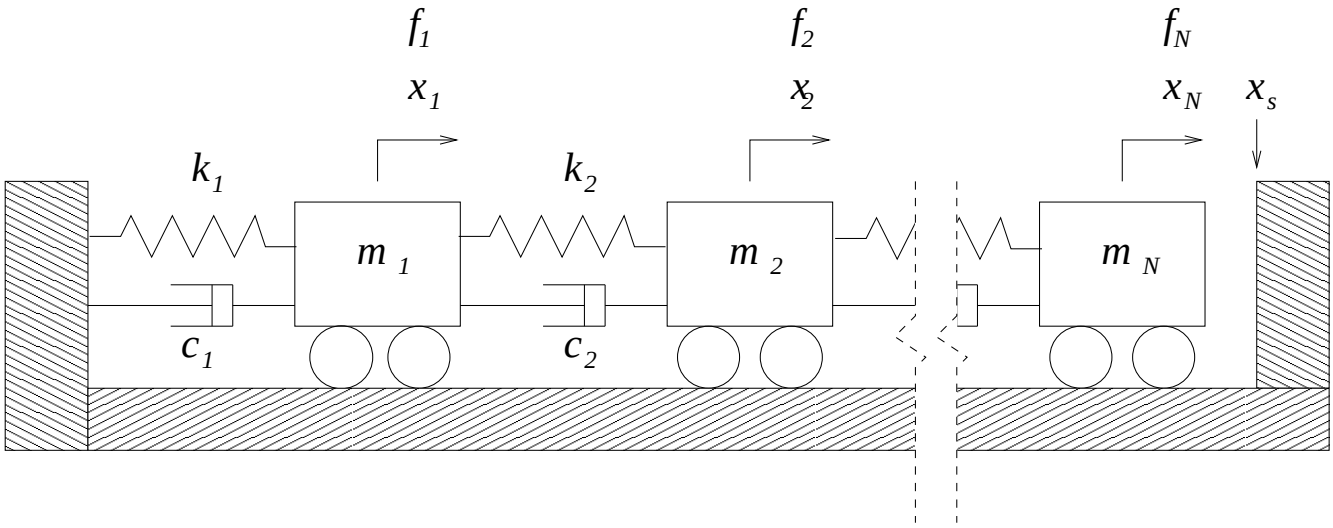

Figure 1:

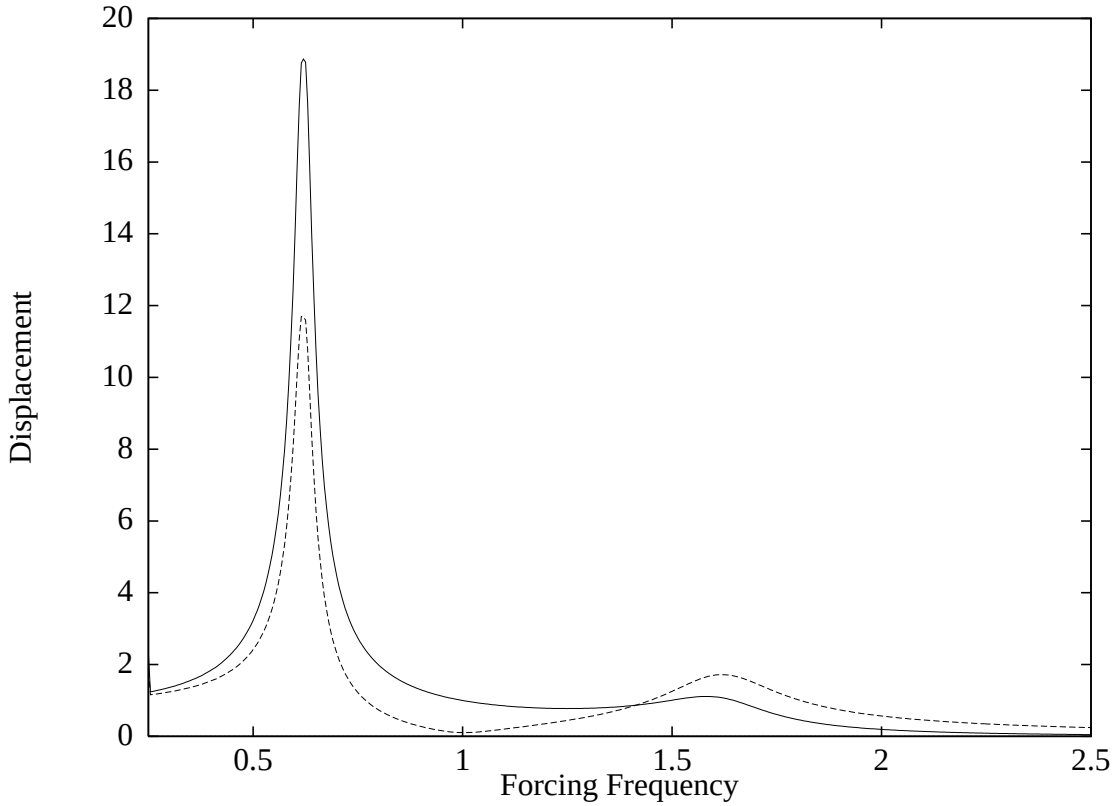
Displacement
Forcing Frequency
0
2
4
6
8
10
12
14
16
18
20
0.5
1
1.5
2
2.5

Figure 2:

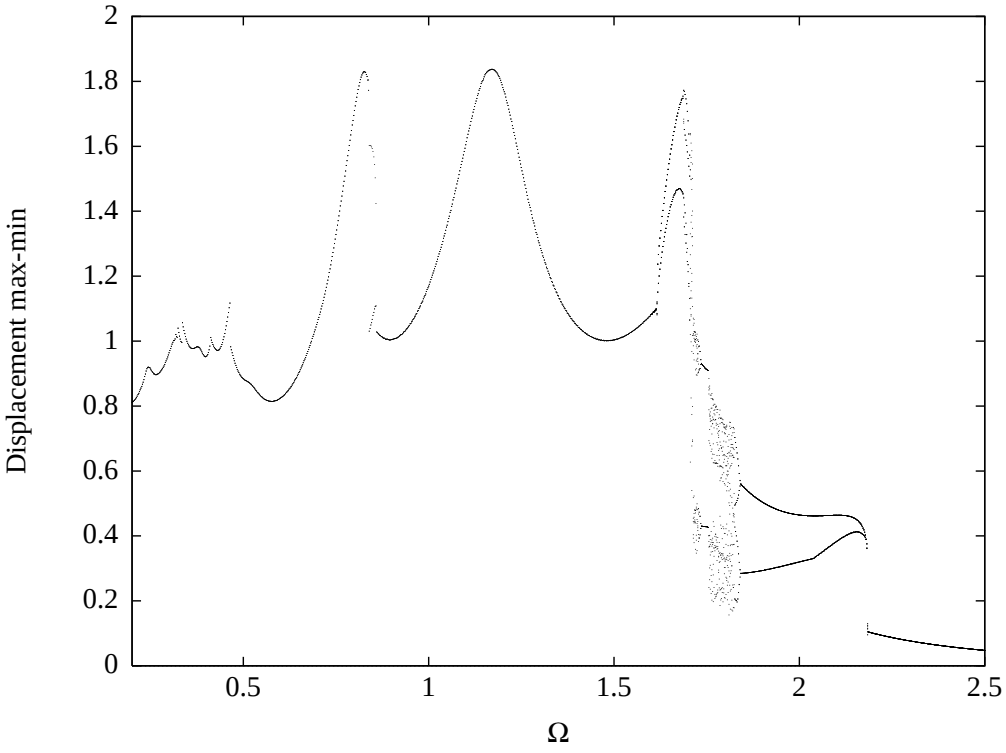
Displacement max-min
Ω
0
0.2
0.4
0.6
0.8
1
1.2
1.4
1.6
1.8
2
0.5
1
1.5
2
2.5

(a)

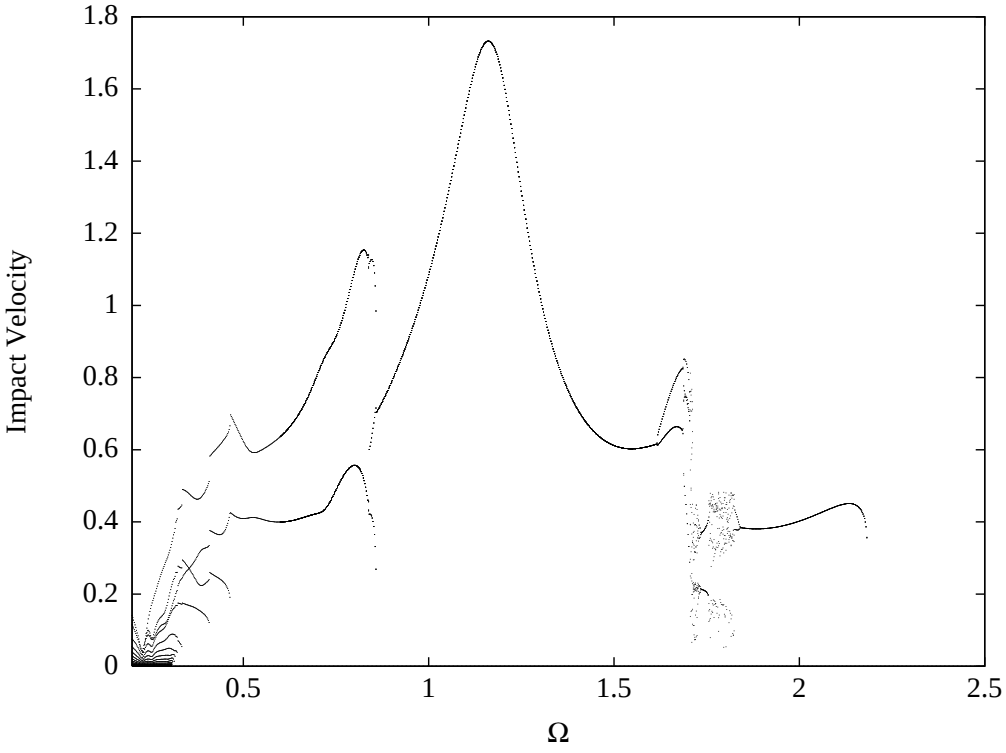
Impact Velocity
Ω
0
0.2
0.4
0.6
0.8
1
1.2
1.4
1.6
1.8
0.5
1
1.5
2
2.5

(b)

Figure 3:

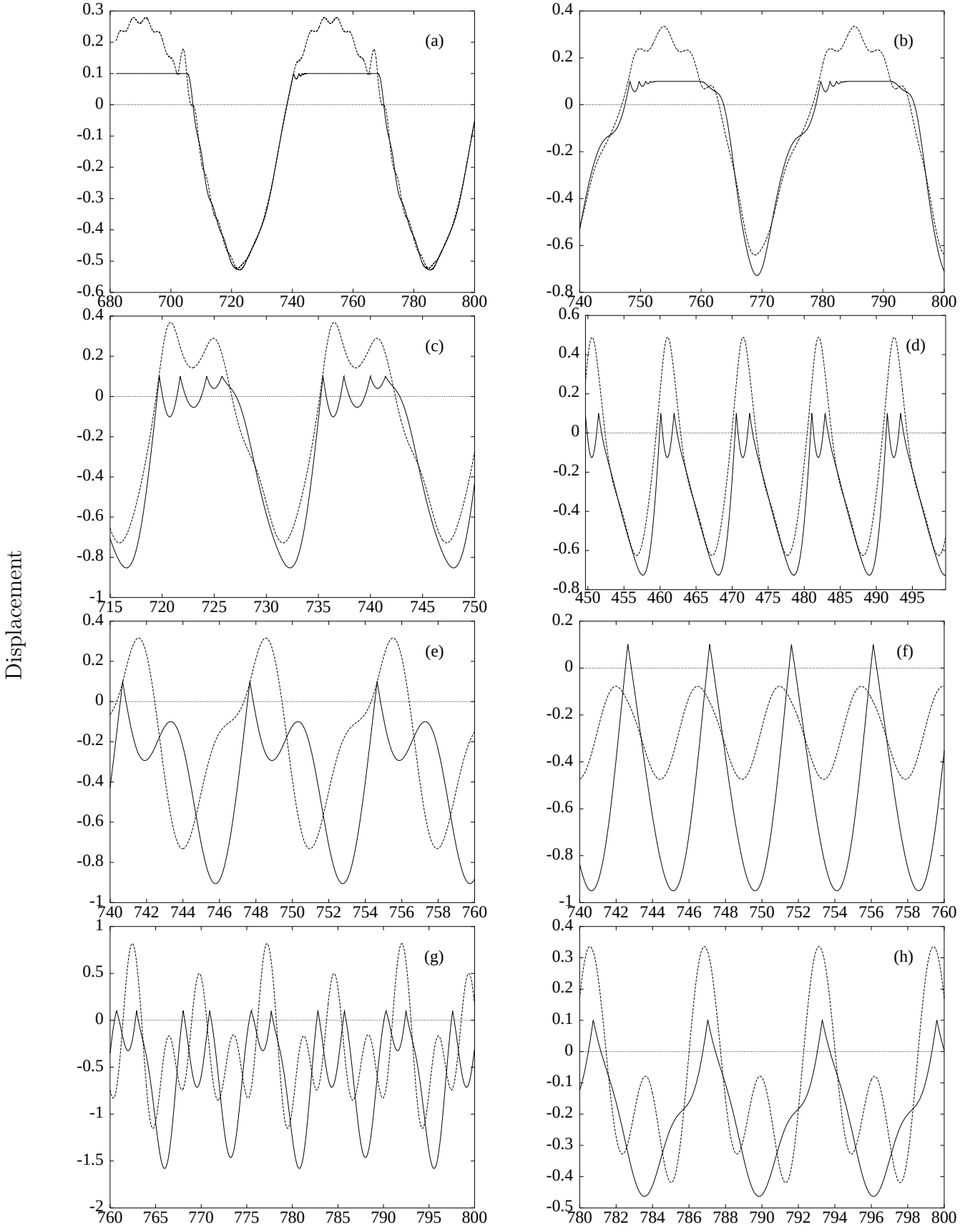

Figure 4:

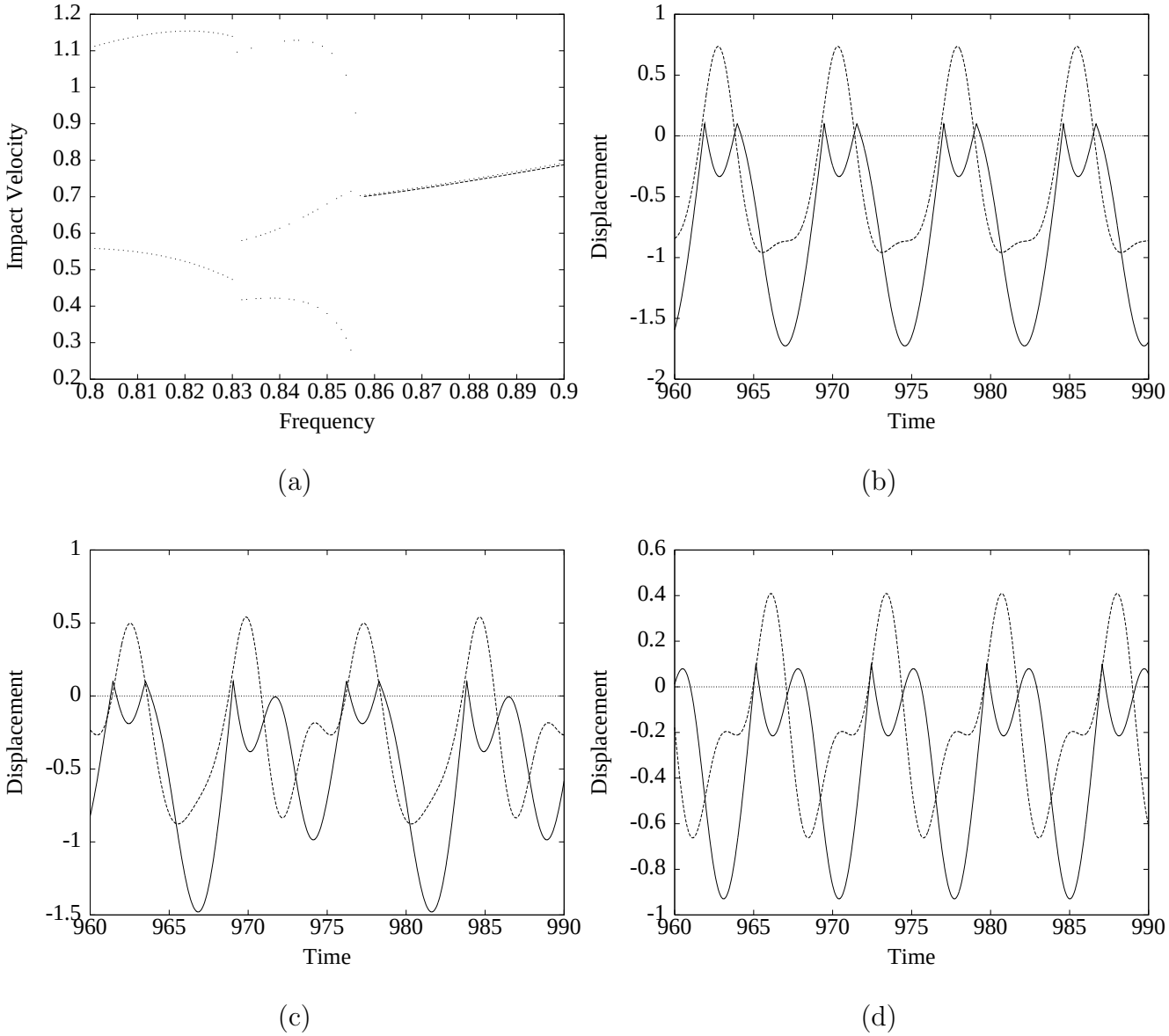

Figure 5:

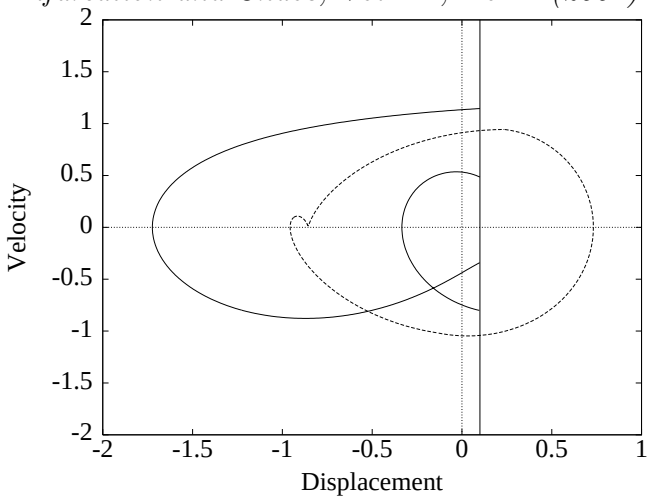
Velocity
Displacement
2
1.5
1
0.5
0
-0.5
-1
-1.5
-2
-2
-1.5
-1
-0.5
0
0.5
1

(a)

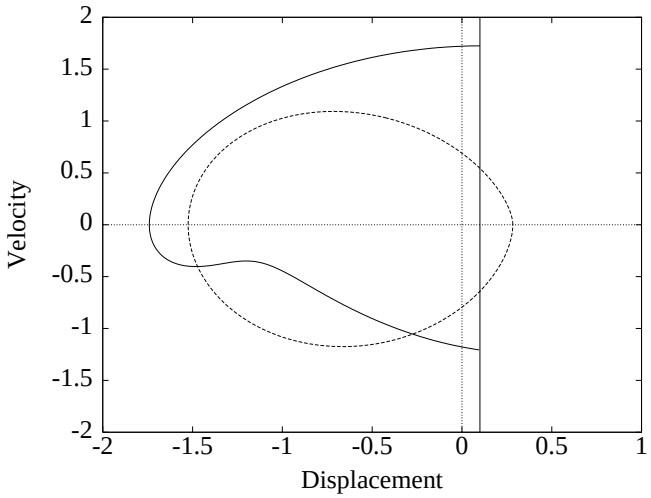
Velocity
Displacement
2
1.5
1
0.5
0
-0.5
-1
-1.5
-2
-2
-1.5
-1
-0.5
0
0.5
1

(b)

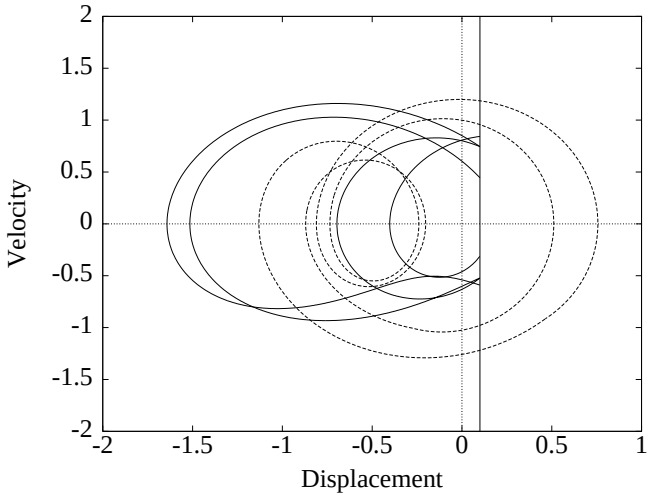
Velocity
Displacement
2
1.5
1
0.5
0
-0.5
-1
-1.5
-2
-2
-1.5
-1
-0.5
0
0.5
1

(c)

Figure 6:

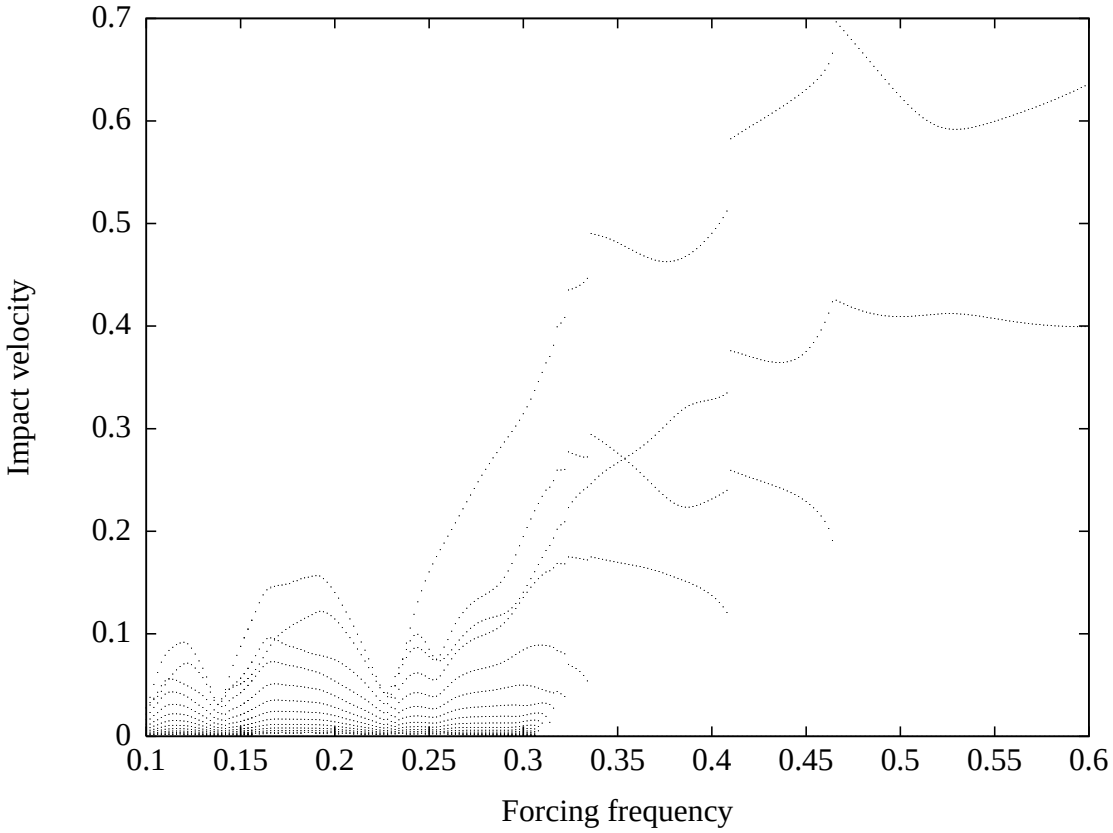
0.7
0.6
0.5
0.4
0.3
0.2
0.1
0
Impact velocity
0.1
0.15
0.2
0.25
0.3
0.35
0.4
0.45
0.5
0.55
0.6
Forcing frequency

Figure 7:

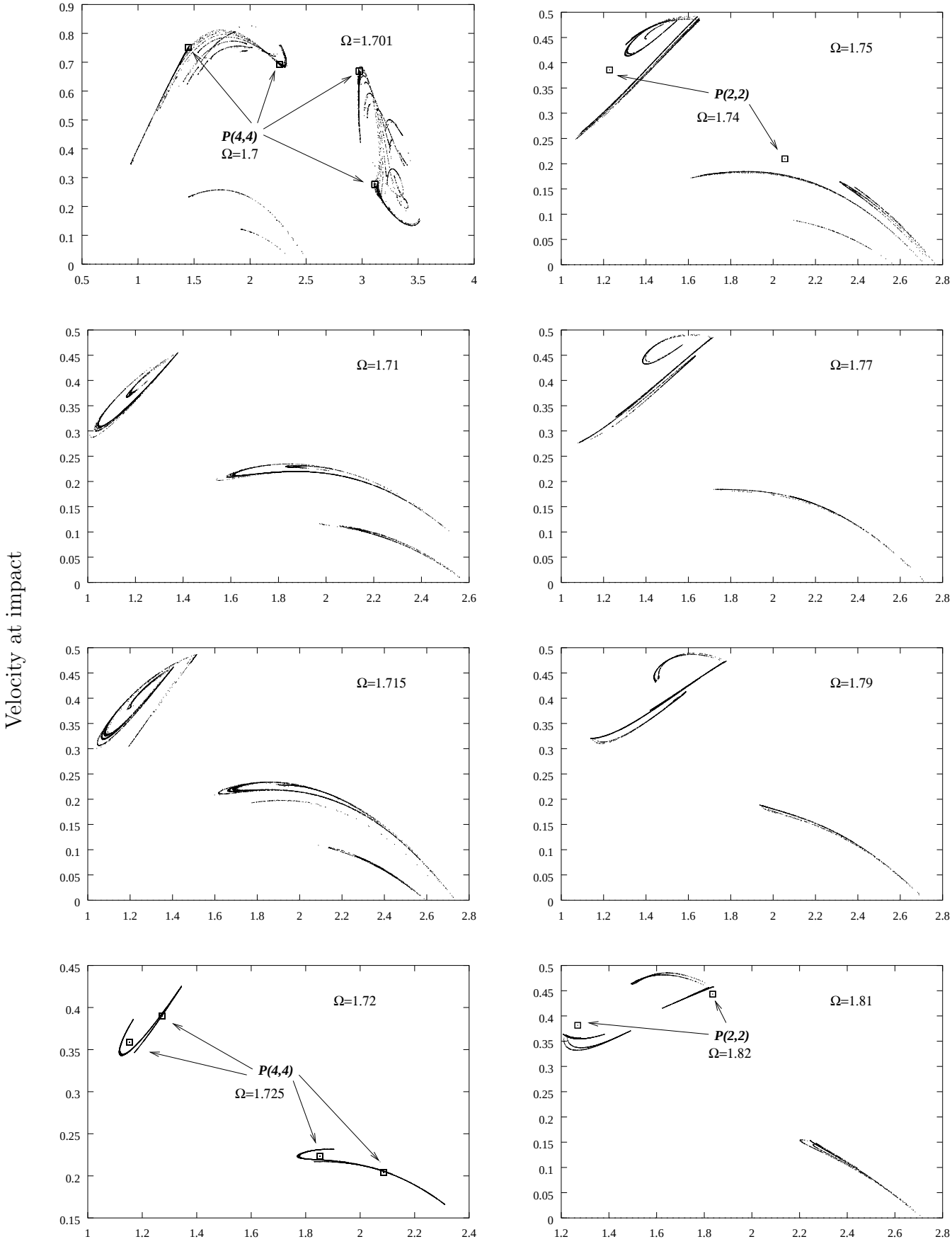
Ω=1.701
P(4,4)
Ω=1.7
Ω=1.75
P(2,2)
Ω=1.74
Ω=1.71
Ω=1.77
Ω=1.715
Ω=1.79
Ω=1.72
P(4,4)
Ω=1.725
Ω=1.81
P(2,2)
Ω=1.82
Velocity at impact
Phase at impact

Figure 8:

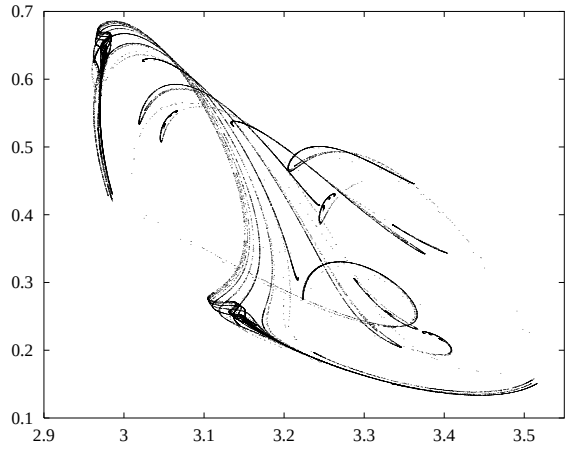

(a)

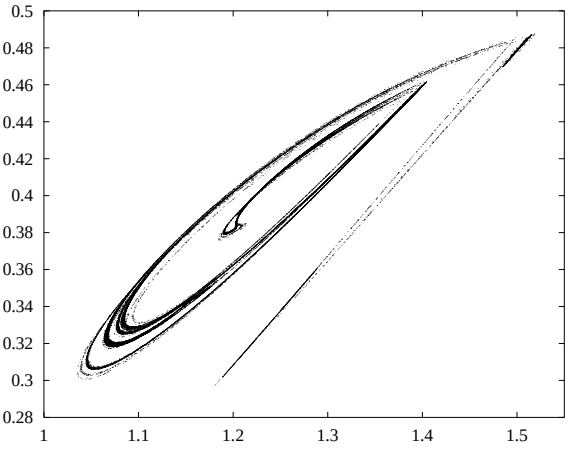

(b)

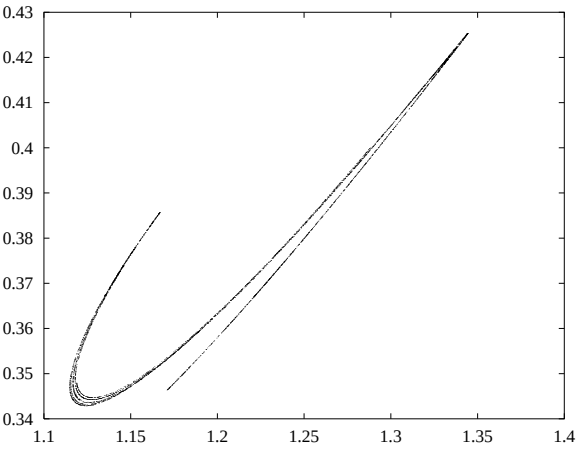

(c)

Velocity at impact

Phase at impact

Figure 9:

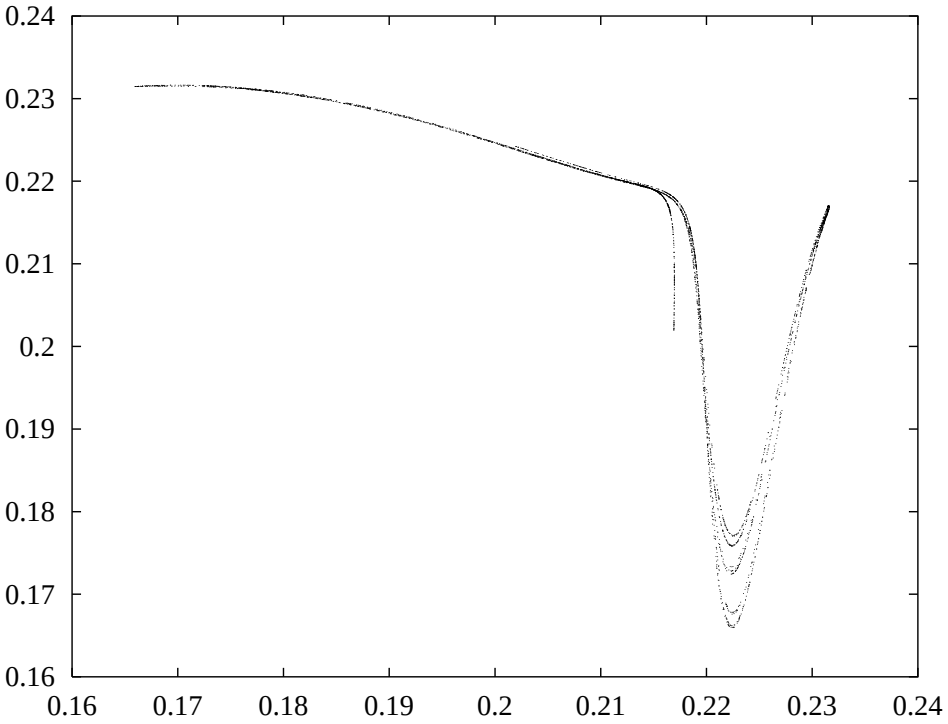

(a)

$v_i(j+1)$

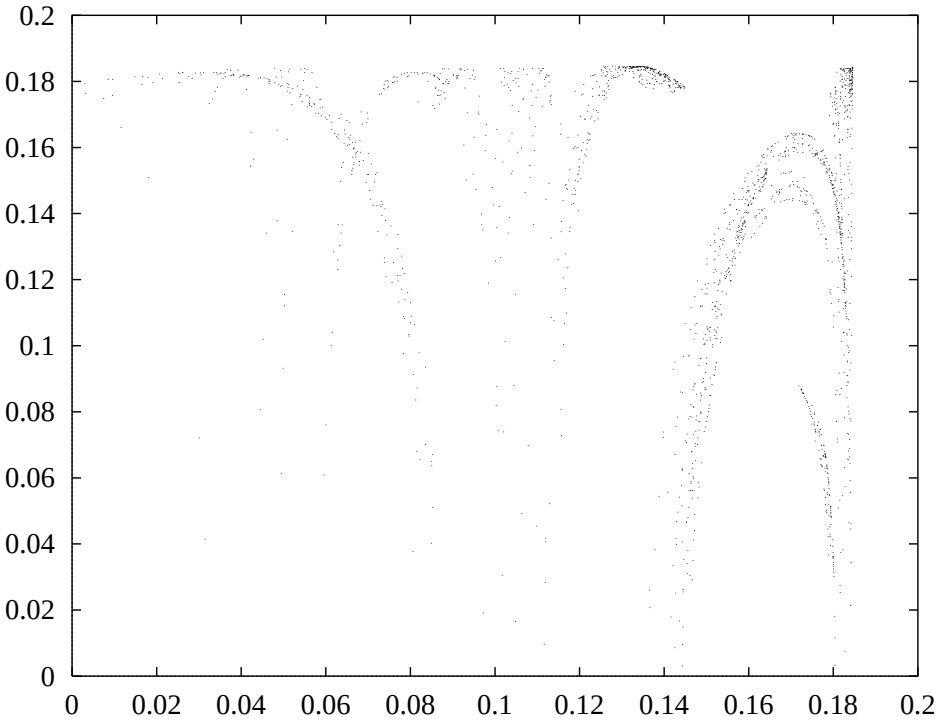

(b)

$v_i(j)$

Figure 10:

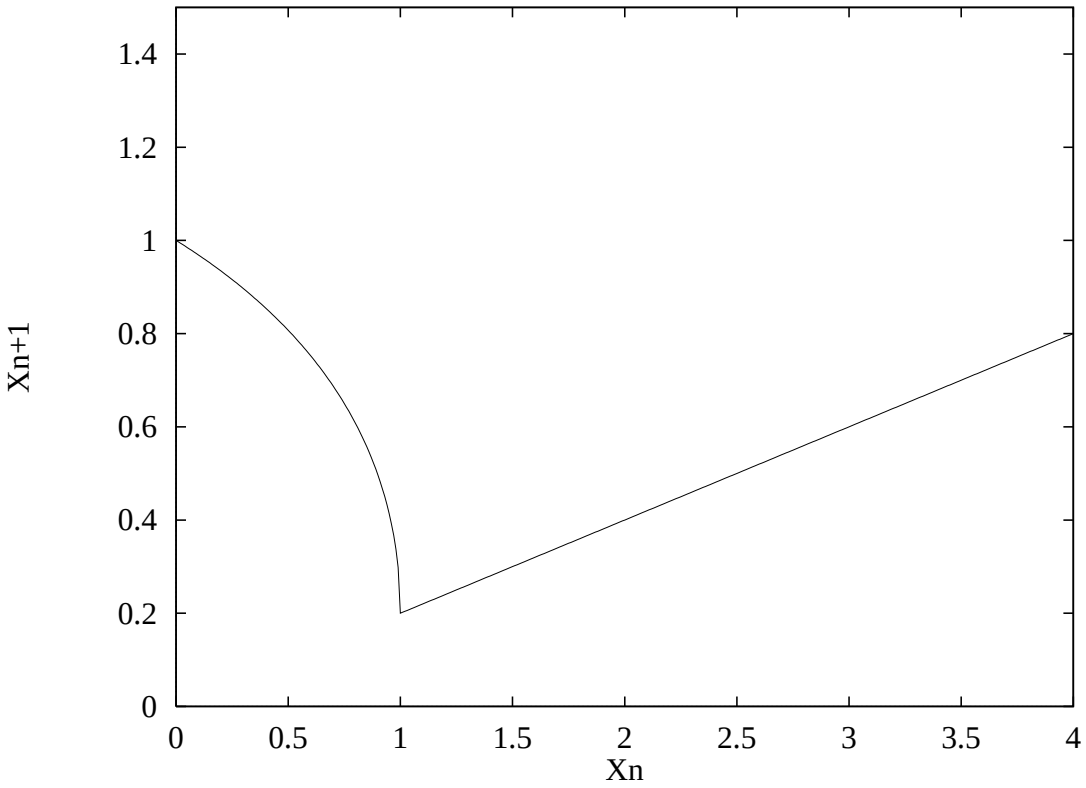

Figure 11:

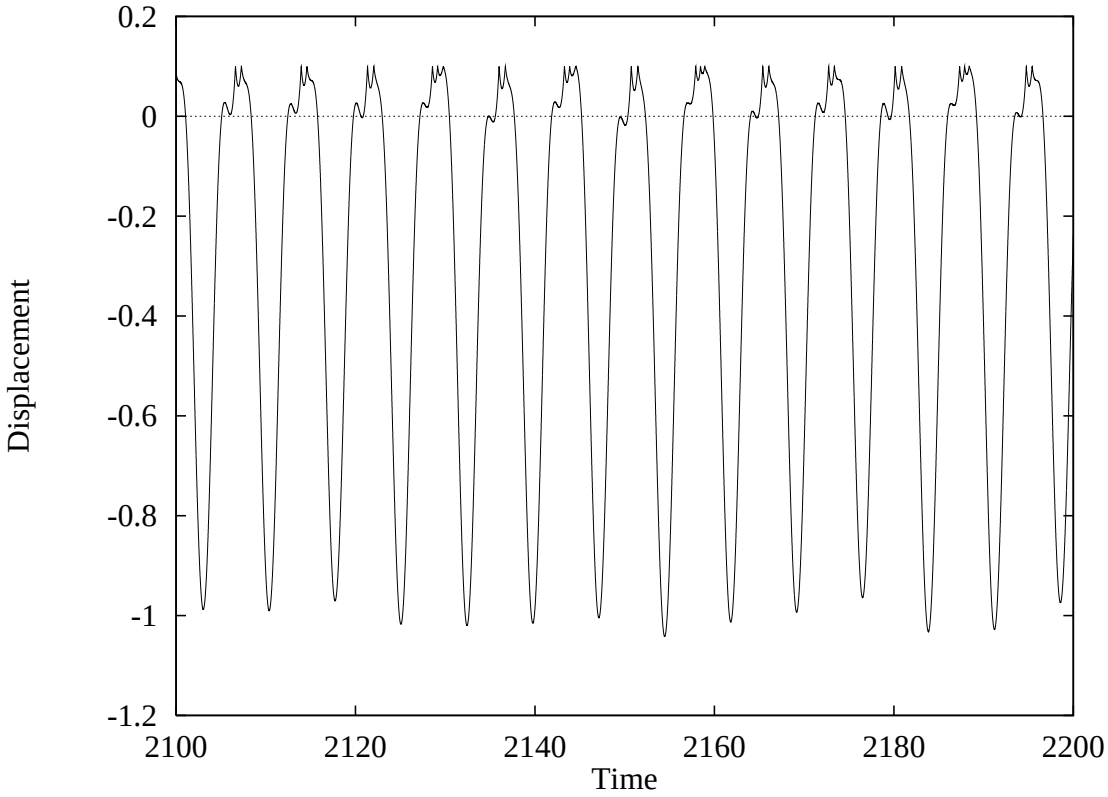
0.2
0
-0.2
-0.4
-0.6
-0.8
-1
-1.2
Displacement
2100
2120
2140
2160
2180
2200
Time

Figure 12: